Stability criteria for the boundary layer formed by throughflow at a horizontal surface of a porous medium

EINDHOVEN UNIVERSITY OF TECHNOLOGY
Department of Mathematics and Computing Science

RANA 01-12
March 2001

Stability criteria for the boundary layer formed by throughflow at a horizontal surface of a porous medium

by

C.J. van Duijn, R.A. Wooding, G.J.M. Pieters, A. van der Ploeg

Reports on Applied and Numerical Analysis
Department of Mathematics and Computing Science
Eindhoven University of Technology
P.O. Box 513
5600 MB Eindhoven, The Netherlands
ISSN: 0926-4507

Stability Criteria for the Boundary Layer Formed by Throughflow at a Horizontal Surface of a Porous Medium

C. J. van Duijn[1], R. A. Wooding[2], G. J. M. Pieters[1], and A. van der Ploeg[3]

We consider gravitational instability of a saline boundary layer formed by evaporation induced throughflow at a horizontal surface of a porous medium. Two paths are followed to analyse stability: the energy method and the method of linearised stability. The energy method requires constraints on saturation and velocity perturbations. The usual constraint is based on the integrated Darcy equation. We give a fairly complete analytical treatment of this case and show that the corresponding stability bound equals the square of the first root of the Bessel function J_0. This explains previous numerical investigations by *Homsy & Sherwood* [1975, 1976]. We also present an alternative energy method using the pointwise Darcy equation as constraint, and we consider the time dependent case of a growing boundary layer. This alternative energy method yields a substantially higher stability bound which is in excellent agreement with the experimental work of *Wooding et al.* [1997a, b]. The method of linearised stability is discussed for completeness because it exhibits a different stability bound. The theoretical bounds are verified by two-dimensional numerical computations. We also discuss some cases of growing instabilities. The presented results have applications to the theory of stability of salt lakes and the salinization of groundwater.

1. INTRODUCTION

Consider a semi-infinite porous medium with a horizontal upper boundary. If a uniform upflow exists within the medium and through the boundary, and if appropriate boundary conditions apply, a spatially one-dimensional boundary layer may be created and sustained by the outflow. For instance, if the surface is maintained at a temperature different from that of the medium and the saturating fluid, a thermal boundary layer is formed with an equilibrium thickness proportional to the ratio of thermal diffusivity to upflow rate. Similarly, a boundary layer is formed by dispersing solute if the solute concentration at the boundary differs from the concentration of the solution issuing from the medium.

Such flows occur naturally in areas of groundwater discharge. These may be characterised by very low flow rates, leading to boundary layers of significant thickness. An upflow of warm or hot groundwater has been postulated for some shallow geothermal areas (*Wooding* [1960]). As the surface is relatively cold, a thermal boundary layer of cool water is formed below the surface. A reversal of this situation relative to gravity may arise for *in situ* coal gasification (*Homsy & Sherwood* [1975]), where a hot reaction surface forms a boundary layer at the lower horizontal boundary of a cooler permeable layer. Boundary layers are also formed in semi-arid regions containing extensive areas of groundwater discharge (*Gilman & Bear* [1996]; *Wooding et al.* [1997a]). The groundwater contains salt. After throughflow induced by evaporation, the salt remains behind at the surface to form saline deposits (salt lakes). These salt lakes may be 'dry' at the surface under the influence of evaporation, or may contain standing water (ponding), perhaps varying seasonally between the two states.

In each of these examples the fluid in the horizontal groundwater boundary-layer differs in density from the fluid in the adjacent permeable medium, and the question of the gravitational stability of the boundary layer arises. *Wooding* [1960] treated the case of a constant-pressure (ponded) boundary by linearised

[1]Department of Mathematics and Computer Science, Eindhoven University of Technology, Eindhoven, The Netherlands
[2]CSIRO Land and Water, Canberra, Australia
[3]MARIN, Wageningen, The Netherlands

stability theory. *Jones & Persichetti* [1986] applied linear analysis to a permeable layer with all combinations of boundary condition and throughflow direction. *Nield* [1987] obtained approximate stability criteria by variational means. *Gilman & Bear* [1996] treated the linearised stability of a horizontal unsaturated layer (vadoze zone) overlying a shallow water table. *Wooding et al.* [1997a, b] discussed saturated groundwater movement with dry or ponded conditions at the surface, and used both experimental and numerical methods to simulate the unstable behaviour of a boundary layer growing from an initial salinity discontinuity at the surface, and including the margin, of a dry salt lake.

In an important step, *Homsy & Sherwood* [1975, 1976] pointed out that the presence of throughflow contributes non-symmetric (odd-order) terms to the stability equations. The linear, time-independent part of the stability equations is not self-adjoint, and linear stability analysis is applicable only when the system is definitely unstable. Subcritical instabilities of finite amplitude are possible at Rayleigh numbers below the critical value derived using linear theory (*Davis* [1971], *Straughan* [1992]).

In the present work we are concerned with this aspect and also with the stability of a growing boundary layer. For simplicity we consider only the dry lake case in a vertical upflow, in which we assume that a rapidly established saturated surface layer exists yielding a steady boundary condition for the salt concentration. We will employ both the energy (variational) method and the method of linearised theory.

1.1. Stability of the Equilibrium Saline Boundary Layer

In applying the energy method we follow two approaches. The first one is the 'standard approach' as outlined, for example, by *Homsy & Sherwood* [1975, 1976] or by *Straughan* [1992]. In this approach one incorporates an integral constraint in the class of admissible perturbations, which is based on continuity and the integrated Darcy equation. The Euler–Lagrange equations with boundary conditions can be combined into a second order eigenvalue problem with time as a parameter. One of the goals of this paper is to demonstrate that at equilibrium, when the boundary layer has reached its large time profile, this eigenvalue problem can be solved in terms of Bessel functions yielding

$$R_{E_1} = 5.7832 \tag{1.1}$$

as a value of the Rayleigh number below which the system is definitely stable; note that $\sqrt{R_{E_1}}$ is the first root of the Bessel function J_0 (*Abramowitz & Stegun* [1972, p. 409]).

In a second approach we deviate from Homsy & Sherwood and consider a different maximum problem. Using the same functional, we replace the integral constraint with an exact differential relation which is now based on continuity and the 'pointwise' Darcy equation. This yields a sixth order eigenvalue problem which we solve numerically by the Jacobi–Davidson method. With the given boundary conditions we find approximately

$$R_{E_2} = 8.590 \tag{1.2}$$

as the largest Rayleigh number below which the system is definitely stable. The close agreement of this result with the numerical results of *Pieters* [2001] and the experimental results of *Wooding et al.* [1997a, b] is discussed in Section 5.

For completeness we also consider the linearised stability analysis of the equilibrium boundary layer. This yields a fourth order eigenvalue problem. Using again the Jacobi–Davidson method we find approximately

$$R_L = 14.35 \tag{1.3}$$

as a critical Rayleigh number above which the system is definitely unstable.

Given the physical parameters of the system a value for the Rayleigh number R_s results. This value may fall within one of three ranges: definitely stable for $R_s \leq R_{E_i}$ $(i = 1, 2)$, definitely unstable for $R_s > R_L$, and possibly unstable to disturbances of finite amplitude (leading to subcritical instabilities) when $R_{E_i} < R_s \leq R_L$.

Homsy & Sherwood [1976] considered throughflow in a finite slab. Their numerical results for large thickness of the slab approximately give the critical Rayleigh numbers (1.1) and (1.3).

1.2. Time Dependent Growth of the Saline Boundary Layer

Problems of fluid instability with impulsively-generated (time-dependent) density profiles have been discussed, in particular, by *Homsy* [1973], who used the energy method to treat global stability of fluid layers, and *Caltagirone* [1980], who compared the stability behaviour using linear and energy methods and also used finite-difference computations for a horizontal porous layer with a sudden rise in surface temperature. These studies, however, did not involve a superimposed throughflow.

Our case involves a dispersive boundary layer in an upflow, and we shall identify approximate parameter

values where instability is likely to occur. Section 3 explains the stability analysis for a growing boundary layer. Here time t appears as a parameter. In the early stages of development, the layer is sufficiently thin to be stabilised by the given boundary conditions. However, the monotonic increase in layer thickness with time will be accompanied by decreasing stability of the system as the influence of the boundary diminishes. This is shown in Figures 2 and 3.

Figure 2 shows a family of curves in the a, R plane, a denoting the horizontal wavenumber, for increasing values of t. The curves are obtained with the energy method based on the differential constraint. For a given time $t > 0$, corresponding to an instantaneous state of the growing boundary layer, let $R_E(t)$ denote the minimum of the corresponding curve. Similarly, Figure 3 shows a family of curves obtained with the linearised stability method. Now, let $R_L(t)$ denote the minimum of the curve corresponding to time t.

We now have the following refinement with respect to the equilibrium case. If $R_s \leq R_E(\infty) = R_{E_2}$, the layer will attain a stable equilibrium profile. If, however, $R_s > R_{E_2}$ we can determine a time t_E^s, corresponding to $R_s = R_E(t_E^s)$, and conclude the stability of the growing boundary layer for $t < t_E^s$. On the other hand, if $R_s > R_L$ we can nominate an elapsed time t_L^s corresponding to $R_s = R_L(t_L^s)$ and conclude the instability of the layer for $t > t_L^s$. These observations follow from the nature of the curves in Figures 2 and 3. The curves in Figure 2 are upper bounds for regions of stable (a, R) combinations, whereas the curves in Figure 3 are lower bounds for regions of unstable (a, R) combinations.

The shape, i.e. number of 'salt-fingers' or critical wavenumber, of growing instabilities depends substantially upon the perturbations present during the initial stable period. This is investigated numerically in Section 4, where we use a finite element approach based on the stream function formulation. If initial perturbations are periodic and sufficiently small we observe growing instabilities in the theoretically predicted range. This is shown in Figure 5 Other perturbations are considered as well. Some qualitative features of the computational results are explained in terms of the stability bounds. In particular the stochastic case meets the theory quite satisfactory (see Section 4.3-a).

In Section 5 we present conclusions and discuss experimental Hele–Shaw results (*Wooding et al.* [1997a, b]) in terms of our theoretical findings. Theory and experiment are reproduced in Figure 6, showing excellent agreement.

The results presented in this contribution are taken from two extensive technical reports, *Van Duijn et al.* [2001] and *Pieters* [2001]. These reports are available upon request from the authors at Eindhoven University of Technology.

2. PROBLEM FORMULATION

Following *Wooding et al.* [1997a], we consider a uniform isotropic porous medium occupying the three dimensional halfspace $\Omega = \{(x, y, z) : -\infty < x, y < \infty,\ z > 0\}$, where z points vertically downwards. The medium is saturated with a fluid of variable density ρ: i.e. water with dissolved salt. Along the upper boundary $\{z = 0\}$ we prescribe density and fluid flow corresponding to a 'dry lake bed', with a sufficient rate of evaporation to remove all free surface water and a rapid buildup of salt. If ρ_r denotes the fluid density in 'natural circumstances' (i.e. far away from the outflow boundary) and ρ_m the maximum density at the outflow boundary, we have $\rho_r \leq \rho \leq \rho_m$ throughout the flow domain Ω.

The flow equations in terms of the Boussinesq approximation (*Bear* [1972], *Nield & Bejan* [1992], *Wooding et al.* [1997a]) are given by:
Fluid incompressibility

$$\text{div } \boldsymbol{q} = 0\,; \tag{2.1}$$

Darcy's law

$$\frac{\mu}{\kappa}\boldsymbol{q} + \text{grad } p - \rho g \boldsymbol{e}_z = \boldsymbol{0}\,; \tag{2.2}$$

Salt transport

$$\phi\frac{\partial \rho}{\partial t} + \text{div } (\rho \boldsymbol{q}) = \mathbb{D}\Delta\rho\,. \tag{2.3}$$

Here $\boldsymbol{q}$ denotes fluid discharge, μ fluid viscosity, κ medium permeability, p fluid pressure, g gravity constant, ϕ porosity and $\mathbb{D}$ an appropriately defined dispersivity or diffusivity. Further, $\boldsymbol{e}_z$ denotes the unit vector in z-direction, pointing downwards.

These equations are considered in Ω subject to the boundary conditions

$$\boldsymbol{q} = -E\boldsymbol{e}_z \quad \text{and} \quad \rho = \rho_m \quad \text{at } z = 0 \tag{2.4}$$

and initial condition

$$\rho|_{t=0} = \rho_r \quad \text{in } \Omega\,. \tag{2.5}$$

Here E denotes the evaporation rate.

We recast the problem in dimensionless form by setting

$$S = \frac{\rho - \rho_r}{\rho_m - \rho_r} \quad \text{and} \quad \boldsymbol{U} = \frac{\boldsymbol{q}}{u_c}, \quad u_c = \frac{(\rho_m - \rho_r) g \kappa}{\mu}, \tag{2.6}$$

and by introducing the scales $\mathbb{D}/E$ and $\phi\mathbb{D}/E^2$, respectively, for length and time. This yields

$$\operatorname{div} \boldsymbol{U} = 0, \tag{2.7}$$

$$\boldsymbol{U} + \operatorname{grad} P - S\boldsymbol{e}_z = \boldsymbol{0}, \tag{2.8}$$

$$\frac{\partial S}{\partial t} + R_s \boldsymbol{U} \cdot \operatorname{grad} S = \Delta S. \tag{2.9}$$

in Ω and for all $t > 0$, subject to

$$\boldsymbol{U} = \boldsymbol{U}_0 := -\frac{1}{R_s}\boldsymbol{e}_z \quad \text{and} \quad S = 1 \quad \text{at } z = 0 \tag{2.10}$$

and

$$S|_{t=0} = 0 \quad \text{in } \Omega. \tag{2.11}$$

Here P denotes an appropriately chosen dimensionless pressure and R_s the system Rayleigh number

$$R_s = \frac{(\rho_m - \rho_r) g \kappa}{\mu E} = \frac{u_c}{E}. \tag{2.12}$$

The main purpose of this paper is to investigate the stability properties of the flow problem defined by (2.7)–(2.12). More specifically, we will consider the stability of the ground-state implied by the uniform initial condition (2.11). Because of the constant boundary data (2.10) this ground-state can be determined explicitly. It is characterized by the uniform upflow

$$\boldsymbol{U} = \boldsymbol{U}_0 \quad \text{in } \Omega \tag{2.13}$$

and the growing boundary layer, for $z > 0$,

$$S = S_0(z,t) = \frac{1}{2}\mathrm{e}^{-z} \operatorname{erfc}\left[\frac{z-t}{2\sqrt{t}}\right] + \frac{1}{2}\operatorname{erfc}\left[\frac{z+t}{2\sqrt{t}}\right], \tag{2.14}$$

satisfying

$$S_0(z,t) \to \mathrm{e}^{-z} \quad \text{as } t \to \infty. \tag{2.15}$$

The corresponding pressure $P = P_0$ is found by integrating Darcy's law (2.8). The stability analysis is based on the expansion

$$S = S_0 + s, \quad \boldsymbol{U} = \boldsymbol{U}_0 + \boldsymbol{u} \quad \text{and} \quad P = P_0 + p, \tag{2.16}$$

with $\boldsymbol{u} = (u, v, w)$, and where S, $\boldsymbol{U}$ and P satisfy equations (2.7)–(2.9) and boundary conditions (2.10). In the next section we study the corresponding perturbation equations. In the analysis we drop the subscript s on R_s and denote the Rayleigh number by R. This is to distinguish between R as an eigenvalue in the equations and its value R_s for the actual physical system.

3. ANALYSIS OF PERTURBATION EQUATIONS

Based on experimental observations of early instabilities we assume that the perturbations are periodic in the horizontal x, y-plane. Further we require

$$s = \boldsymbol{u} = 0 \quad \text{at } z = 0, \infty, \tag{3.1}$$

expressing that $\{S, \boldsymbol{U}\}$ and $\{S_0, \boldsymbol{U}_0\}$ both satisfy (2.10) and behave similarly at large depth.

3.1. Perturbation Equations

Substituting (2.16) into equations (2.7)–(2.9) and writing R instead of R_s, yields the system (in Ω and for all $t > 0$)

$$\operatorname{div} \boldsymbol{u} = 0, \tag{3.2}$$

$$\boldsymbol{u} + \operatorname{grad} p - s\boldsymbol{e}_z = \boldsymbol{0}, \tag{3.3}$$

$$\frac{\partial s}{\partial t} - \frac{\partial s}{\partial z} + Rw\frac{\partial S_0}{\partial z} + R\boldsymbol{u} \cdot \operatorname{grad} s = \Delta s. \tag{3.4}$$

As in *Lapwood* [1948] we note that equations (3.2) and (3.3) can be combined to give for s and w the linear relation

$$\Delta w = \Delta_\perp s \quad \text{in } \Omega, \tag{3.5}$$

where $\Delta_\perp$ denotes the horizontal Laplacian

$$\frac{\partial^2}{\partial x^2} + \frac{\partial^2}{\partial y^2}.$$

This relation plays a crucial role in various parts of the stability analysis.

Because of the assumed x, y periodicity, we may restrict the analysis of equations (3.2)–(3.4) to the periodicity cell

$$\mathcal{V} = \{(x,y,z) : |x| < \pi/a_x, \ |y| < \pi/a_y, \ 0 < z < \infty\}, \tag{3.6}$$

where a_x and a_y are the, as yet unspecified, horizontal wavenumbers. We call

$$a := \sqrt{a_x^2 + a_y^2} \tag{3.7}$$

the horizontal wavenumber of the periodicity cell $\mathcal{V}$.

There are two well-known paths to carry out the stability analysis: the variational energy method and the method of linearised stability. Some important references in this respect are *Wooding* [1960], *Nield* [1987], *Straughan* [1992] and *Homsy & Sherwood* [1976]. Because of the existing throughflow ($\boldsymbol{U} = \boldsymbol{U}_0$), the energy method and the linearized stability method yield different stability bounds on the Rayleigh number. Therefore we will discuss both approaches.

3.2. Energy Method

In the energy method one estimates the time derivative of the L^2-norm of the saturation perturbation. In particular, the aim is to find the largest Rayleigh number for which

$$\frac{\mathrm{d}}{\mathrm{d}t}\int_{\mathcal{V}} s^2 < 0\,. \tag{3.8}$$

The value of R for which this inequality is satisfied clearly will depend on the wavenumber a and, because $S_0 = S_0(z,t)$, on time t. Once (3.8) is established, it follows that the L^2-norm of the velocity perturbation is bounded as well, since (*Van Duijn et al.* [2001])

$$\int_{\mathcal{V}} |\boldsymbol{u}|^2 \le \int_{\mathcal{V}} s^2\,. \tag{3.9}$$

This is a direct consequence of (3.2) and (3.3).

To investigate (3.8), we multiply (3.4) by s and integrate over $\mathcal{V}$. Using (3.2) we find the identity

$$\frac{\mathrm{d}}{\mathrm{d}t}\frac{1}{2}\int_{\mathcal{V}} s^2 = -\int_{\mathcal{V}} |\mathrm{grad}\ s|^2 - R\int_{\mathcal{V}} sw\frac{\partial S_0}{\partial z}\,. \tag{3.10}$$

Thus if R is chosen such that the right-hand side of (3.10) is negative for all perturbations satisfying a given constraint, then stability is guaranteed.

It is our aim to investigate the consequences of two different constraints. In the first we consider perturbations satisfying (3.2) and the integrated Darcy equation:

$$\int_{\mathcal{V}} |\boldsymbol{u}|^2 - \int_{\mathcal{V}} sw = 0\,. \tag{3.11}$$

This approach is a modification of that used by *Homsy & Sherwood* [1976]. While they considered a stationary ground state only and solved the corresponding eigenvalue problem numerically, we are in the position to deal with time evolution of the primary profile as well. However, we shall not pursue the time dependence for this constraint. Instead we give a complete analytical treatment of the case where the ground state is given by (2.15) for all $t > 0$. This analysis explains quite elegantly some of the previously obtained numerical results.

In the second constraint, we consider perturbations satisfying the differential expression (3.5). We shall treat the time dependent ground state and show that this differential constraint significantly improves integral constraint (3.11).

3.2.1. Integral constraint. Identity (3.10) and constraints (3.2), (3.11) lead to the maximum problem

$$\frac{1}{R} = \sup_{(s,\boldsymbol{u})\in\mathbf{H}} \frac{-\int_{\mathcal{V}} \frac{\partial S_0}{\partial z} sw}{\int_{\mathcal{V}} |\mathrm{grad}\ s|^2} \tag{3.12}$$

with

$$\mathbf{H} = \big\{(s,\boldsymbol{u}) : x,y\text{-periodic with respect to } \mathcal{V},\ s = \boldsymbol{u} = 0 \text{ at } z = 0,\infty,\ \mathrm{div}\ \boldsymbol{u} = 0 \text{ and } \int_{\mathcal{V}} |\boldsymbol{u}|^2 = \int_{\mathcal{V}} sw\big\}\,.$$

The corresponding Euler–Lagrange equations are

$$\begin{cases} -2\Delta s + R\dfrac{\partial S_0}{\partial z} w - \mu w = 0\,, \\ 2\mu\boldsymbol{u} - \mathrm{grad}\ \pi + R\dfrac{\partial S_0}{\partial z} s\boldsymbol{e}_z - \mu s\boldsymbol{e}_z = \boldsymbol{0}\,, \\ \mathrm{div}\ \boldsymbol{u} = 0 \quad \text{and} \quad \displaystyle\int_{\mathcal{V}} |\boldsymbol{u}|^2 = \int_{\mathcal{V}} sw\,, \end{cases}$$

where μ (constant in space) and π are Lagrange multipliers. Applying the scaling

$$\boldsymbol{u} := \frac{\lambda}{\sqrt{R}}\boldsymbol{u}\,, \quad \mu = \frac{R}{\lambda^2} \quad \text{and} \quad p = -\frac{1}{2}\frac{\lambda}{\sqrt{R}}\pi\,,$$

one finds

$$\begin{cases} \dfrac{\sqrt{R}}{2}\left(\dfrac{1}{\lambda} - \lambda\dfrac{\partial S_0}{\partial z}\right) w + \Delta s = 0\,, & (3.13) \\ \dfrac{\sqrt{R}}{2}\left(\dfrac{1}{\lambda} - \lambda\dfrac{\partial S_0}{\partial z}\right) s\boldsymbol{e}_z - \boldsymbol{u} - \mathrm{grad}\ p = \boldsymbol{0}\,, & (3.14) \\ \mathrm{div}\ \boldsymbol{u} = 0\,, & (3.15) \\ \displaystyle\int_{\mathcal{V}} |\boldsymbol{u}|^2 = \frac{\sqrt{R}}{\lambda}\int_{\mathcal{V}} sw\,. & (3.16) \end{cases}$$

These equations were also found by Homsy & Sherwood with a slightly different interpretation of the parameter λ. Note that (3.14) has a structure similar to Darcy's

law.

As before, (3.14) and (3.15) can be combined to give

$$\Delta w = \frac{\sqrt{R}}{2}\left(\frac{1}{\lambda} - \lambda\frac{\partial S_0}{\partial z}\right)\Delta_\perp s\,. \tag{3.17}$$

Further, multiplying (3.14) by u, integrating the result over $\mathcal{V}$, and using (3.16) yields the useful identity

$$\lambda^2 = \frac{\int_{\mathcal{V}} sw}{-\int_{\mathcal{V}} \frac{\partial S_0}{\partial z} sw}\,. \tag{3.18}$$

Finally, multiplying (3.13) by s, integrating the result over $\mathcal{V}$, and using (3.18) gives

$$\int_{\mathcal{V}} |\mathrm{grad}\ s|^2 = \frac{\sqrt{R}}{\lambda}\int_{\mathcal{V}} sw\,. \tag{3.19}$$

Next we introduce the periodicity. Setting $s := as$, with a given by (3.7), we find from (3.13) and (3.17) the equations (with D signifying $\mathrm{d}/\mathrm{d}z$)

$$\left(D^2 - a^2\right)s + \frac{a\sqrt{R}}{2}\left(\frac{1}{\lambda} - \lambda\frac{\partial S_0}{\partial z}\right)w = 0\,, \tag{3.20}$$

$$\left(D^2 - a^2\right)w + \frac{a\sqrt{R}}{2}\left(\frac{1}{\lambda} - \lambda\frac{\partial S_0}{\partial z}\right)s = 0\,, \tag{3.21}$$

for $0 < z < \infty$. Note that in these equations t appears as a parameter through the ground state. We seek nontrivial solutions subject to the homogeneous conditions (3.1) and the constraint (3.18).

As a first observation we note that (3.20), (3.21) and the boundary conditions imply $s = w$. Hence we are left with the second order boundary value problem (for $0 < z < \infty$)

$$\begin{cases} \left(D^2 - a^2\right)s + \dfrac{a\sqrt{R}}{2}\left(\dfrac{1}{\lambda} - \lambda\dfrac{\partial S_0}{\partial z}\right)s = 0\,, & (3.22)\\ s(0) = s(\infty) = 0\,, & (3.23) \end{cases}$$

subject to the constraint (replacing w by s in (3.18))

$$\lambda^2 = \frac{\int_0^\infty s^2}{-\int_0^\infty \frac{\partial S_0}{\partial z} s^2}\,. \tag{3.24}$$

Identity (3.19) rewrites into

$$\int_0^\infty (Ds)^2 = \left(\frac{\sqrt{R}a}{\lambda} - a^2\right)\int_0^\infty s^2\,. \tag{3.25}$$

This expression and equation (3.22), using $\dfrac{\partial S_0}{\partial z} \to 0$ as $z \to \infty$, imply that nontrivial solutions only exist in the parameter range

$$1 < \frac{\sqrt{R}}{a\lambda} < 2\,. \tag{3.26}$$

So far we have not used the explicit form of S_0. In the analysis below we confine ourselves to the equilibrium case (2.15), where S_0 is a simple decaying exponential. Introducing the new parameters

$$\delta = \frac{\sqrt{R}}{a\lambda} \quad (\text{with } 1 < \delta < 2)\,, \quad \alpha = \sqrt{\frac{2R}{\delta}}\,,$$

$$\beta = \beta(a,\delta) = 2a\sqrt{1 - \frac{\delta}{2}}\,, \tag{3.27}$$

and the transformation

$$\xi = \alpha \mathrm{e}^{-z/2}\,, \quad f(\xi) = s(z)\,, \tag{3.28}$$

we find for f a boundary value problem involving the Bessel equation

$$\xi^2 f'' + \xi f' + (\xi^2 - \beta^2)f = 0 \quad \text{on } 0 < \xi < \alpha\,, \tag{3.29}$$

with

$$f(0) = f(\alpha) = 0\,. \tag{3.30}$$

Here primes denote differentiation with respect to ξ. A solution of (3.29) satisfying the first condition in (3.30) is

$$f(\xi) = J_\beta(\xi)\,, \tag{3.31}$$

with J_β denoting the Bessel function of the first kind, order β. Next we fix $a > 0$ and consider

$$J_{\beta(a,\delta)}(\xi_1) = 0 \quad \text{for } 1 < \delta < 2\,, \tag{3.32}$$

where $\xi_1 = \xi_1(a,\delta)$ is the first positive zero of J_β. Then setting $\alpha = \xi_1$ in the second equation of (3.27), we obtain the first eigenvalue R_1 for the given values of a and δ:

$$R_1 = R_1(a,\delta) = \frac{1}{2}\delta\left(\xi_1(a,\delta)\right)^2 \quad \text{for } 1 < \delta < 2\,. \tag{3.33}$$

Keeping a fixed, we now turn to the integral constraint (3.24). In the transformed variables it reads

$$\frac{1}{\delta} = 2a^2\frac{\int_0^{\xi_1}\frac{1}{\xi}J_\beta^2(\xi)\mathrm{d}\xi}{\int_0^{\xi_1}\xi J_\beta^2(\xi)\mathrm{d}\xi}\,. \tag{3.34}$$

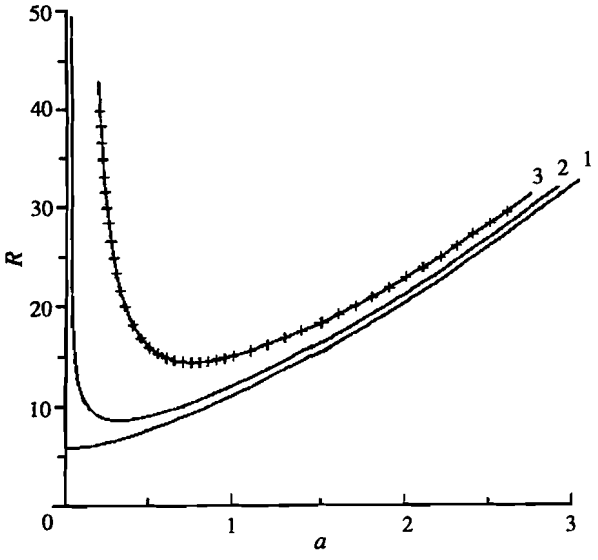

Figure 1. Comparison of estimates involving lowest eigenvalue R_1 versus wavenumber a for the equilibrium boundary layer. Curve 1: Energy method using integral constraint. Curve 2: Energy method using differential constraint. Curve 3: Linearised stability method using Jacobi–Davidson (solid curve) and Frobenius expansion (crossed points).

The question now arises whether there exists a unique number $\delta_a \in (1,2)$ such that $\delta = \delta_a$ satisfies (3.34). This would result in the first eigenvalue

$$R_1(a) := R_1(a, \delta_a) \quad \text{for } a > 0\,. \tag{3.35}$$

The proof involves some technical details which are given in *Van Duijn et al.* [2001]. The energy stability curve in the a, R-plane is plotted as curve 1 in Figure 1. If perturbations are x, y-periodic with wavenumber a and if $R_s < R_1(a)$, then the ground state (at equilibrium) is stable in the L^2-sense. The construction implies

$$R_1(0) = \lim_{a \downarrow 0} R_1(a) = 5.784\cdots \quad \text{(first zero of } J_0)\,. \tag{3.36}$$

Homsy & Sherwood used a numerical shooting method to solve the eigenvalue problem. They found (3.36) approximately as a stability bound.

3.2.2. Differential constraint. In a second approach we want to achieve (3.8) for perturbations satisfying the diffential constraint (3.5). This leads to a maximum problem in which (3.12) is considered for the space of perturbations

$$\widetilde{\mathbf{H}} = \big\{(s,w) : x,y\text{-periodic with respect to } \mathcal{V},\ s = w = 0 \text{ at } z = 0,\infty, \text{ and } \Delta w = \Delta_\perp s \text{ in } \mathcal{V}\big\}\,.$$

This maximum problem results in an eigenvalue problem which has a much higher complexity than the eigenvalue problem related to (3.11). In fact it leads to a sixth order differential equation in terms of w, for which no explicit solution is known. However, one expects to have a more accurate description, yielding larger Rayleigh numbers, in particular since (3.5) is based on the pointwise Darcy equation. This statement is made precise in Appendix A.

Now the Euler–Lagrange equations read (*Van Duijn et al.* [2001]):

$$\left(D^2 - a^2\right) s = \frac{R}{2}\frac{\partial S_0}{\partial z} w + \frac{a^2}{2}\pi\,, \tag{3.37}$$

$$\left(D^2 - a^2\right) \pi = -R\frac{\partial S_0}{\partial z} s\,, \tag{3.38}$$

with $\pi(0) = 0$ as natural boundary condition, and

$$\left(D^2 - a^2\right) w = -a^2 s\,. \tag{3.39}$$

These equations need to be solved for $0 < z < \infty$ and they contain time t (through $S_0 = S_0(z,t)$) as parameter. Eliminating π from equations (3.37) and (3.38) yields a fourth order equation in s and w, and the further elimination of s using (3.39) leads to the sixth order w equation

$$\left(D^2 - a^2\right)^3 w + \frac{a^2 R}{2}\left\{\left(D^2 - a^2\right)\left(\frac{\partial S_0}{\partial z} w\right) + \frac{\partial S_0}{\partial z}\left(D^2 - a^2\right) w\right\} = 0\,. \tag{3.40}$$

The corresponding boundary conditions for this equation are

$$w(\infty) = 0\,, \tag{3.41}$$

implying that all higher order derivatives vanish as well at $z = \infty$, and

$$w(0) = D^2 w(0) = D^4 w(0) = 0\,. \tag{3.42}$$

The first two conditions are obvious. The third one is a consequence of $\pi(0) = 0$; this condition implies $D^2 s(0) = 0$ from (3.37), which is then used in (3.39). In terms of the variables w, s and π, we have the homogeneous conditions

$$w = s = \pi = 0 \quad \text{at} \quad z = 0, \infty\,. \tag{3.43}$$

The eigenvalue problem (3.40), (3.41) and (3.42), or equivalently (3.37)–(3.39) subject to (3.43), was solved numerically by the Jacobi–Davidson method. This method is briefly described in *Van Duijn et al.* [2001]. Detailed information is given in *Fokkema et al.* [1999] and *Sleijpen & Van Der Vorst* [1996].

For a given wavenumber $a > 0$ and time $t > 0$, let $R_E(a,t)$ denote the smallest positive eigenvalue. The dashed curves in Figure 2 show the numerical approximations of the curves $\{(a,R) : a > 0,\ R = R_E(a,t)\}$ for increasing values of t. Note that these curves essentially move downwards, except for large a and t. At large time they converge to the equilibrium curve, corresponding to (2.15). This limit case is also shown in Figure 1 (curve 2). The results obtained with the differential constraint are superior to the results obtained with the integral constraint. In particular, the minimum of curve 2 is $R = 8.590$ approximately, which is significantly higher than the minimum of about $R = 5.78$ of curve 1.

To interpret the results of the time dependent case, we set

$$R_E(t) := \min_{a>0} R_E(a,t) \quad \text{for } 0 < t < \infty \tag{3.44}$$

and we recall the Rayleigh number of the physical system R_s, given by (2.12).

If $R_s < R_E(\infty) =: R_E$, which we denoted by R_{E_2} in the introduction, the boundary layer is definitely stable for all $t > 0$. However, if $R_s > R_E$, we can only conclude that the boundary layer is stable for $0 < t < t_E^s$, where t_E^s is determined by $R_s = R_E(t_E^s)$. When $t > t_E^s$ no direct conclusions can be drawn. The appearance and form of the growing instabilities critically depends on the choice of initial perturbations. This is further investigated in Section 4.

3.3. Linearised Stability

In the method of linearised stability one disregards the higher order terms in (3.4) and considers the approximate linear saturation equation

$$\frac{\partial s}{\partial t} - \frac{\partial s}{\partial z} + Rw\frac{\partial S_0}{\partial z} = \Delta s \quad \text{in } \Omega \tag{3.45}$$

for $t > 0$. We shall seek nontrivial solutions of this equation together with (3.5), subject to the homogeneous boundary conditions (3.1). In case of a stationary ground state one looks for solutions having an exponential growth rate in time. Since here, the ground state depends on time as well, such a construction is only possible under the assumption that the rate of change

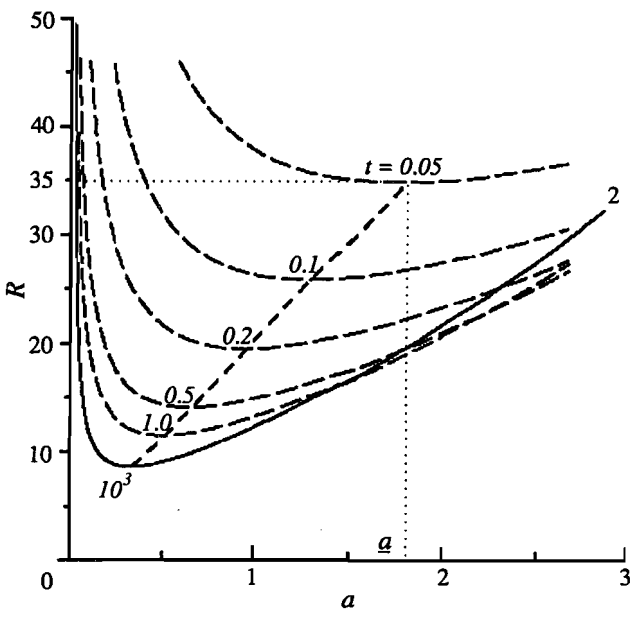

Figure 2. Solid curve: Stability curve for equilibrium boundary layer according to the energy method with differential constraint. Dashed curves: Stability curves prior to equilibrium. Numerical values are calculated by the Jacobi–Davidson method. Short-dashed curve traces minima of stability curves with increasing $t > 0$.

of the ground state is small compared with the growth rate of infinitesimal perturbations (the frozen profile approach). Hence, for given $t > 0$, we consider instead of (3.45) the approximate equation

$$\frac{\partial s}{\partial \tau} - \frac{\partial s}{\partial z} + Rw\frac{\partial S_0}{\partial z}(t,z) = \Delta s \quad \text{in } \Omega \tag{3.46}$$

for $\tau > 0$ and sufficiently small. Now again t appears as a parameter in the equation, as in the case of the energy methods. From here on the procedure is quite standard (*Wooding* [1960], *Nield & Bejan* [1992]). Applying again the x, y periodicity, taking σ as the exponential growth rate and setting

$$s, w = s, w(z) \exp\left(\sigma\tau + i(a_x x + a_y y)\right) , \tag{3.47}$$

we find from (3.5) and (3.46) the coupled set of second order equations

$$\begin{cases} \left(D^2 - a^2\right) w = -a^2 s , & (3.48) \\ \left(D^2 + D - a^2 - \sigma\right) s = R\dfrac{\partial S_0}{\partial z}(z,t) w . & (3.49) \end{cases}$$

The corresponding eigenvalues now depend on a, t and on the growth rate σ. In Appendix B we show for the

smallest positive eigenvalue $R_1(a,t,\sigma)$:

$$R_1(a,t,\sigma) \lesseqgtr R_1(a,t,0) \text{ if and only if } \sigma \lesseqgtr 0\,. \quad (3.50)$$

These inequalities imply the following. Let R_s be sufficiently close to $R_1(a,t,0)$. If $R_s > R_1(a,t,0)$, then there exists a $\sigma > 0$ such that $R_s = R_1(a,t,\sigma)$. In other words, if $R_s > R_1(a,t,0)$, there exists a growing infinitesimal perturbation which implies that the boundary layer is unstable. If $R_s < R_1(a,t,0)$ no definite statement about stability can be made. Only certain infinitesimal perturbations now decay. Others, and in particular large perturbations, may still grow in time.

As a consequence it suffices to analyse equations (3.48), (3.49) for the case of neutral stability $\sigma = 0$. Eliminating s and setting $\sigma = 0$, gives for w the fourth order eigenvalue problem

$$\left(D^2 + D - a^2\right)\left(D^2 - a^2\right) w = -a^2 R \frac{\partial S_0}{\partial z}(z,t) w \quad (3.51)$$

for $0 < z < \infty$, with

$$w(0) = D^2 w(0) = 0 \quad \text{and} \quad w(\infty) = 0\,. \quad (3.52)$$

The equilibrium case ($t = \infty$ and $S_0 = \mathrm{e}^{-z}$) can be treated by a semi-analytical technique based on a Frobenius expansion in terms of descending exponentials (*Van Duijn et al.* [2001], *Wooding* [1960]). As a result one finds an accurate approximation to the lowest eigenvalue $R_1(a)$ for any wavenumber $a > 0$. In Figure 1, point values of $R_1(a)$ have been plotted as crosses, showing excellent agreement with solid curve 3 – the numerical solution of the eigenvalue problem (3.51), (3.52) using the Jacobi–Davidson method. We find

$$R_L := \min_{a>0} R_1(a) = R_1(a_c) = 14.35 \quad (3.53)$$

with

$$a_c = 0.759 \quad (3.54)$$

approximately. These numbers, in good agreement with the numerical results of *Homsy & Sherwood* [1976], are characteristic of the linearised stability method.

To study the instability of the growing boundary layer we need to consider the eigenvalue problem for each finite $t > 0$. Let $R_L(a,t)$ denote the smallest positive eigenvalue. Again we used the Jacobi–Davidson method to find accurate numerical approximations. These results are shown in Figure 3 where the dashed curves indicate $R_L(a,t)$ for increasing values of t. Note again

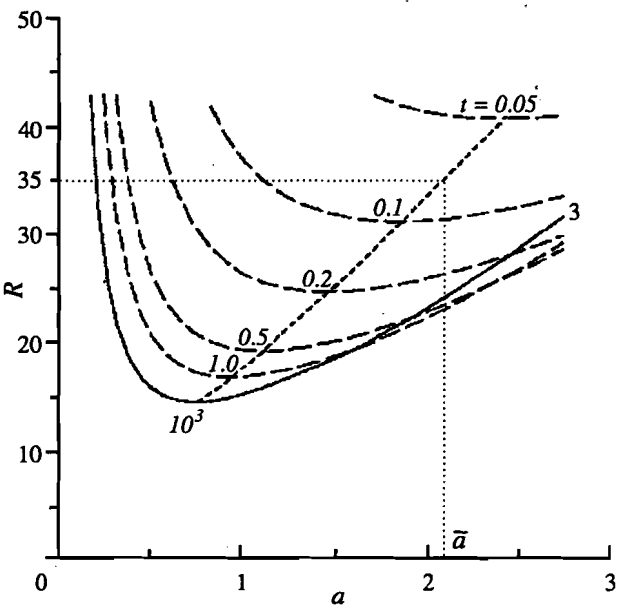

Figure 3. Solid curve: Stability curve for equilibrium boundary layer according to linearised stability method. Dashed curves: Estimate of stability curves prior to equilibrium, treating time as parameter. Numerical values are calculated by the Jacobi–Davidson method.

that these curves essentially move downwards, except for large a and t. As $t \to \infty$ convergence towards the equilibrium curve $R_1(a)$ is attained.

As before, we set

$$R_L(t) := \min_{a>0} R_L(a,t)\,. \quad (3.55)$$

If $R_s > R_L(\infty) =: R_L$, an estimate for the onset time of instability is found by the crossover time t_L^s determined by $R_s = R_L(t_L^s)$. In other words, the boundary layer becomes unstable for $t > t_L^s$. If $R_s \approx R_L$, the boundary layer becomes unstable when it is close to its equilibrium profile.

For $R_s < R_L$ no definite statement about stability is possible. The linearised stability analysis only implies that infinitesimal small perturbations vanish for $R_s < R_L$. Subcritical instabilities originating from large perturbations may still grow in time. This is a consequence of the uniform upflow, implying that the eigenvalue problem is not self-adjoint (*Homsy & Sherwood* [1976]).

4. GROWING INSTABILITIES

The theoretical stability bounds tell us how the system will respond to periodic perturbations of the initial

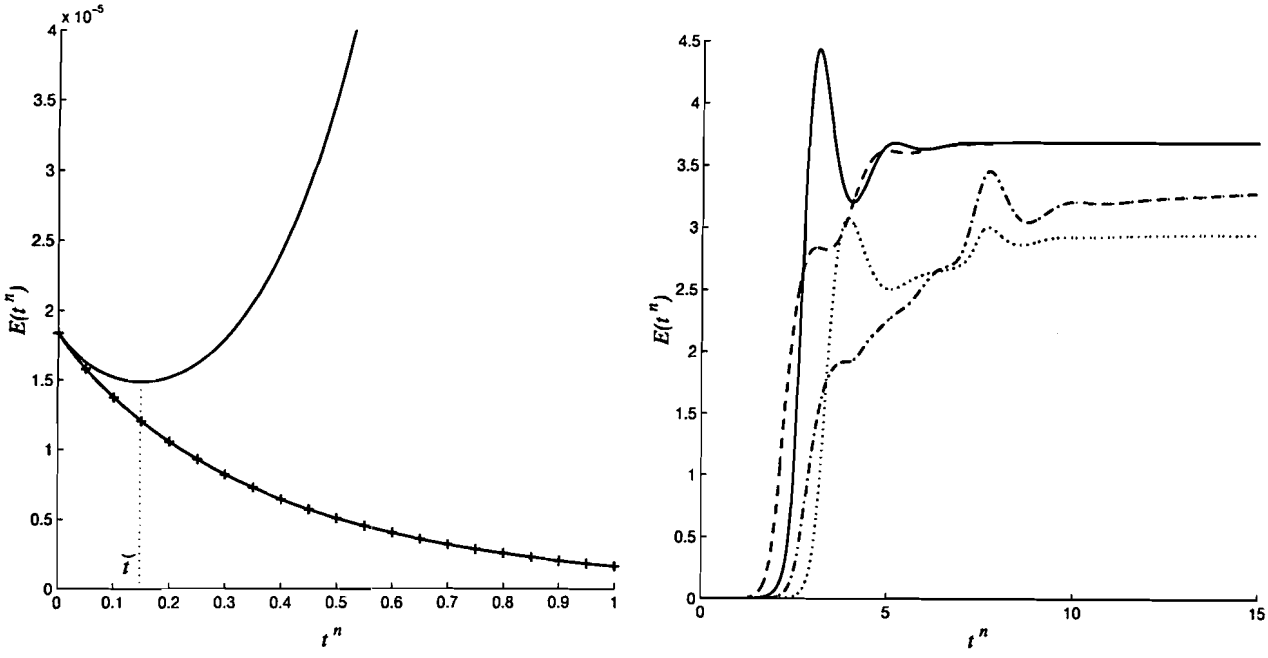

Figure 4. Left: Early-time behaviour of $E(t^n)$ originating from (4.8): solid line ($R_s = 35$), crossed solid line ($R_s = 5$). Right: Long-time behaviour of energy $E(t^n)$ for $R_s = 35$. Solid line corresponds to perturbation (4.8), dotted line to (4.9), dash-dot line to (4.10) and finally dashed line to (4.11).

state $S = 0$. For $R_s < R_E$ we expect decaying perturbations and for $R_s > R_L$ growing instabilities or salt-fingers. In this section we verify this behaviour by means of numerical experiments. We also investigate the response of the system to non-periodic (Plates 2,3) and a combination of periodic (Plate 4) initial perturbations.

In the numerical experiments we consider the two-dimensional truncated flow domain

$$\Omega_H^L := \{(x,z) : -L < x < L,\ 0 < z < H\}\,. \qquad (4.1)$$

In this definition the quantities H and L are scaled with respect to the length scale $\mathbb{D}/E$. The truncated flow domain needs additional boundary conditions for the velocity $\boldsymbol{U}$ and the saturation S: we set $S = 0$ and $\boldsymbol{U} = \boldsymbol{U}_0$ at $z = H$ and we impose no-flow and no salt transport along the lateral boundaries.

We solve equations (2.7)–(2.9) in terms of the saturation S and the stream function Ψ, where

$$\boldsymbol{U} = \operatorname{curl}\Psi := \left(-\frac{\partial\Psi}{\partial z}, \frac{\partial\Psi}{\partial x}\right)\,. \qquad (4.2)$$

Following *de Josselin de Jong* [1960] we obtain the system

$$\begin{cases} \dfrac{\partial S}{\partial t} + R_s\left(\dfrac{\partial\Psi}{\partial x}\dfrac{\partial S}{\partial z} - \dfrac{\partial\Psi}{\partial z}\dfrac{\partial S}{\partial x}\right) = \Delta S\,, & (4.3)\\ \Delta\Psi = \dfrac{\partial S}{\partial x}\,, & (4.4) \end{cases}$$

in Ω_H^L and for all $t > 0$. The corresponding boundary conditions result directly from the imposed saturation and flow behaviour.

4.1. The Numerical Method

Let $t^n = n\Delta t$, $n = 1, 2, \cdots, N$, N sufficiently large, and let S^n denote the saturation at $t = t^n$. The corresponding stream function is found from

$$\Delta\Psi = \frac{\partial S^n}{\partial x} \quad \text{in } \Omega_H^L\,. \qquad (4.5)$$

This problem is discretised by the finite (linear) element method. The corresponding matrix equation is iteratively solved using the conjugate gradient method. The numerical approximation of (4.5) is denoted by Ψ_h^n.

Next we consider

$$\frac{\partial S}{\partial t} + R_s\left(\frac{\partial\Psi_h^n}{\partial x}\frac{\partial S}{\partial z} - \frac{\partial\Psi_h^n}{\partial x}\frac{\partial S}{\partial x}\right) = \Delta S\,, \qquad (4.6)$$

in Ω_H^L and for $t > t^n$. Again we use a finite element discretisation, together with an upwind discretisation for the convective part. Now the corresponding linear system is iteratively solved with the bi-conjugate gradient stabilized method. For the time integration we use the implicit Euler scheme. The numerical solution of (4.6) is denoted by S_h^{n+1}. Replacing S^{n+1} in equation (4.5) by the approximation S_h^{n+1}, the above cycle is repeated for subsequent time steps.

The numerical method does not involve automatic time-step adaptation nor does it include algorithms for local mesh refinement. This implies that the time-step and mesh are fixed during the computations. The mesh consists of square elements of length h. Motivated by the convergence behaviour of the scheme (see *Pieters* [2001] for technical details), we use $\Delta t = 0.005$ and $h = 0.15625$ for respectively the time-step and element length, and we fix $H = 5$ and $L = 25$.

4.2. Stability Criterion

To decide whether the system is stable or unstable, a stability criterion is required. Inspired by the energy method we consider the functional

$$E(t^n) := \int_{\Omega_H^L} |\boldsymbol{u}_h^n(x,z,t)|^2 \,\mathrm{d}x\mathrm{d}z\,, \qquad (4.7)$$

where $\boldsymbol{u}_h^n$ is the numerical approximation of the velocity perturbation $\boldsymbol{u}$. It is found by substracting the ground state $\boldsymbol{U}_0$ from the numerical solution $\boldsymbol{U}_h^n = \mathrm{curl}\, \Psi_h^n$.

Numerical observations (*Pieters* [2001]) show that $E(t^n)$ either decreases from a positive value $E(0)$ towards zero for large n, or $E(t^n)$ first decreases, reaches a minimum and then strongly increases away from $E(0)$. Based on these observations, we call the ground state unstable if there exists a $m \in \mathbb{N}$ such that $E(t^m) \leq E(t^n)$ for all $0 \leq n \leq N$. Otherwise the ground state is stable. The time t^m is called turning time and will be further denoted by $\breve{t}$.

The behaviour of $E(t^n)$ is illustrated by two numerical experiments. First we set $R_s = 5 < R_E$ and consider

$$S(x,z,t=0) = \epsilon\cos(x)\,, \qquad \epsilon = 5\cdot 10^{-4}\,, \qquad (4.8)$$

for $(x,z) \in \Omega_H^L$. The functional (4.7) is plotted as a crossed solid line in Figure 4 (left). Indeed, for this choice the energy norm decreases with time and the system remains stable. Next we set $R_s = 35 > R_L$ and again (4.8). For this unstable regime the functional is plotted as solid curves in Figure 4. The saturation profile and velocity field for this experiment are depicted in Plate 1. As to be expected, the initial periodic perturbation triggers growing instabilities in the saturation profile. At later times the influence of the lower boundary becomes noticeable (middle and bottom figures) and a steady state is reached. The corresponding saturation profile has the original eight fingers. This is due to the particular choice $a = 1$. Note that the energy $E(t^n)$ has a relative high value, Figure 4 (right).

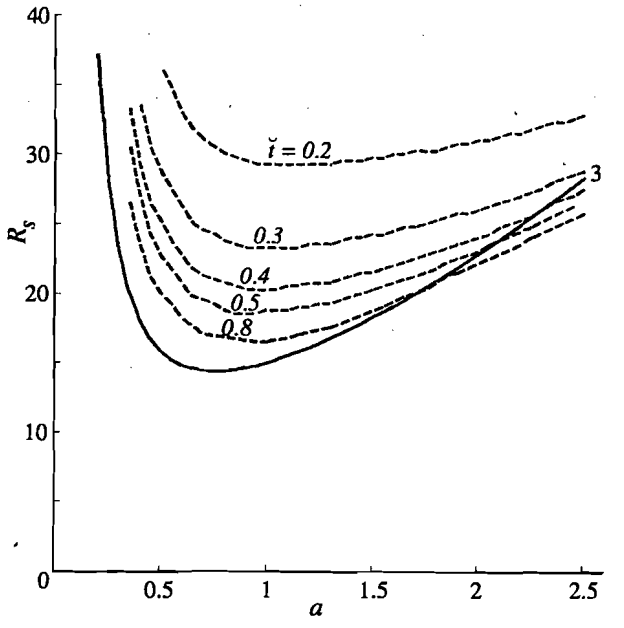

Figure 5. Solid curve: Stability curve for equilibrium boundary layer according to linearised stability method. Dashed curves: Stability curves treating $\breve{t}$ as parameter.

As explained in *Pieters* [2001] this observation leads to an alternative method to analyse stability of the system: given wavenumbers a and Rayleigh numbers R_s within relevant ranges, we can determine the turning times $\breve{t}$, yielding a set of triples $(a, R_s, \breve{t})$. Treating $\breve{t}$ as parameter, we can construct stability curves similar to the ones in Section 3. The result is shown in Figure 5 and agrees with the curves obtained by the method of linearised stability (Figure 3). This is due to the fact that the initial perturbations are small.

4.3. Numerical Experiments

We investigate the development of instabilities for more general initial perturbations. We take $R_s = 35$ and consider the following cases:

a. Stochastic perturbation, with

$$S(x,z,t=0) = \epsilon\mu(x,z)\,, \quad \text{for } (x,z) \in \Omega_H^L\,, \qquad (4.9)$$

where μ is uniformly distributed in $[0,1]$.

The computational results are shown in Plate 2. The

system clearly selects a preferential wavenumber a^* for small and intermediate times. From the top figure in Plate 2 we deduce $a^* = 1.86$ approximately. At later times a steady state is reached which now has a saturation profile with twelve fingers and a relative low energy.

Taking $R_s = 35$ and considering the curve connecting the minima in Figure 3, we expect to find from linear stability $a = \overline{a} = 2.08$. Similarly, we obtain from the energy method, Figure 2, $a = \underline{a} = 1.82$. We observe that $\underline{a} \approx a^* < \overline{a}$. This is in agreement with the experimental results of *Wooding et al.* [1997a, b], see also Figure 6 in Section 5.

b. Non-periodic perturbation, with

$$S(x,z,t=0) = \begin{cases} \epsilon & \text{for } -\frac{L}{3} < x < \frac{L}{3},\ 0 < z < H\,, \\ 0 & \text{elsewhere}\,, \end{cases} \tag{4.10}$$

The results for flow and saturation are shown in Plate 3. Now, at small and intermediate times, no preferential wave number can be detected. At large times the resulting steady state shows ten fingers and an intermediate energy $E(t^n)$. We stopped the computations at $t = 15$. It could be possible that the steady state is not yet reached because the corresponding energy is still slightly increasing in time.

c. Combination of periodic perturbations, with

$$S(x,z,t=0) = \epsilon\{\cos(0.25x) + \cos(x) + \cos(2x)\}\,, \tag{4.11}$$

for $(x,z) \in \Omega_H^L$.

We observe that the modes with $a = 0.25$, 2 decay, while the one with $a = 1$ grows. The decay of $a = 0.25$ is in agreement with the stability analysis (Figure 3). However, Figures 2 and 3 seem to indicate competition between $a = 1$ and $a = 2$. Apparently, nonlinear effects cause decay of $a = 2$ and growth of $a = 1$. Note that the large time behaviour is identical to Plate 1, with the same energy.

5. DISCUSSION AND CONCLUSIONS

We have formulated a stability problem involving a porous medium saturated with saline water flowing vertically upwards through a horizontal surface. The upflowing water is assumed to evaporate completely at the surface. Salt saturation is established quickly and is sustained there, with excess salt precipitated on the surface. Below the surface, a saline boundary layer grows by diffusion in the counter direction to the upflow. If this layer remains stable under gravity, an equilibrium state is reached where the salinity (or density) profile is exponential, decreasing downwards towards the ambient upflow value.

Since the surface salinity and upflow rate are both taken constant, the layer is stable provided it is sufficiently thin; it is initially stable, but will tend to become less stable monotonically as the thickness increases by diffusion/dispersion. The system is least stable when the boundary layer has attained maximum thickness, which occurs at equilibrium. The equilibrium boundary-layer thickness provides a length scale for the Rayleigh instability problem. If the porous medium has a lower boundary, it is assumed to be at a distance large relative to that scale.

To study the stability of the boundary layer we have used two energy methods and the method of linearised stability. In terms of the system Rayleigh number R_s (2.12), the first give upperbounds for stability, the latter a lower bound for unstable behaviour. These bounds do not coincide (see Figure 1) and leave the possibility for decay of infinitesimal small perturbations and growth of large perturbations.

In the first energy method we follow *Homsy & Sherwood* [1976] and use (3.11) as constraint for perturbations. Assuming horizontal periodicity in the usual way, this constraint leads to a second order eigenvalue problem. Homsy and Sherwood constructed a numerical solution for the case of a porous layer of finite thickness with a (thermal) boundary layer at equilibrium. We explain their asymptotic result for large thickness in terms of Bessel functions. In particular we find that their stability bound corresponds to the square of the first root of the Bessel function J_0.

In the second energy method we use (3.5) as differential constraint and we consider the time dependent behaviour (growth) of the boundary layer. This leads to a sixth order eigenvalue problem which we solved by means of the Jacobi–Davidson method. Figure 2 shows the behaviour of the smallest positive eigenvalue versus the wavenumber a, with time as parameter. Figure 1 compares the two methods for the equilibrium case ($t = \infty$) and shows superior behaviour when using (3.5) instead of (3.11). This is explained in Appendix A. Given a R_s-value, we are now in a position to estimate the time during which the boundary layer grows in a stable manner. This is explained in Section 3.2.2, see (3.44).

The method of linearised stability estimates the onset of instabilities. We used the frozen profile approach which allows us to incorporate the growth of the boundary layer in the analysis. As a result we arrive at a

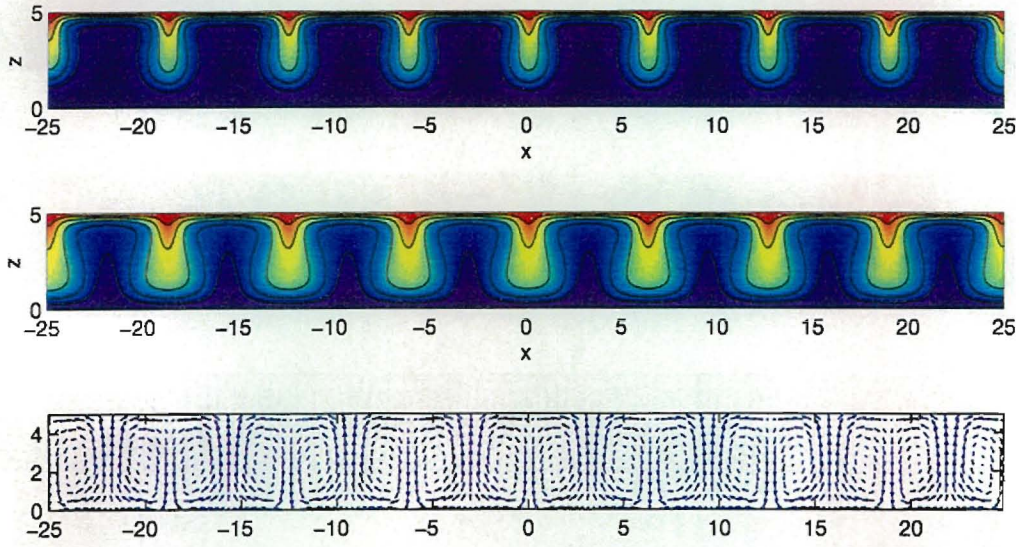

Plate 1. Periodic initial perturbation (4.8): saturation profile at $t = 3$ (top) and $t = 15$ (middle), velocity field (bottom) at $t = 15$.

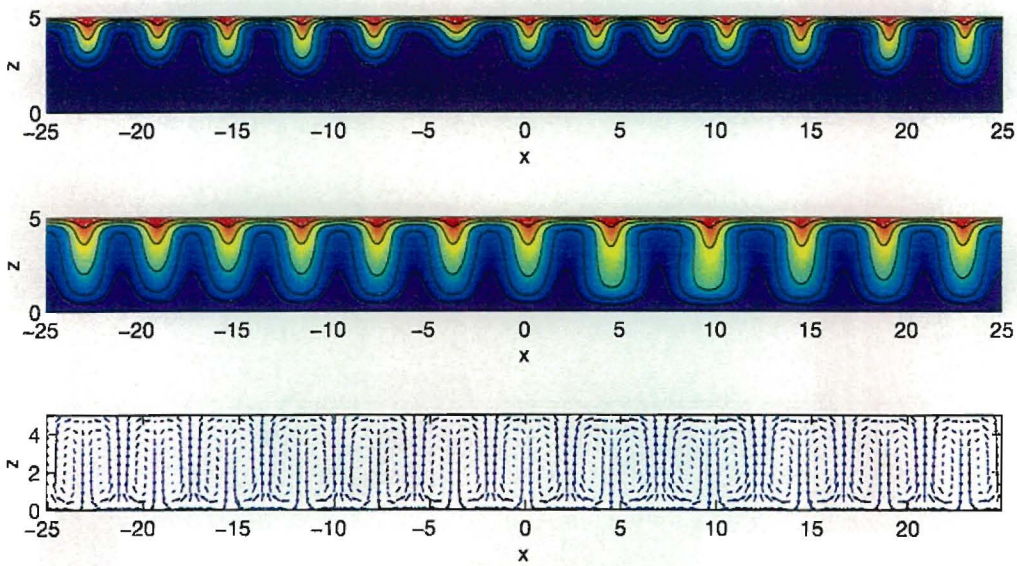

Plate 2. Stochastic initial perturbation (4.9): saturation profile at $t = 3.5$ (top) and $t = 15$ (middle), velocity field (bottom) at $t = 15$.

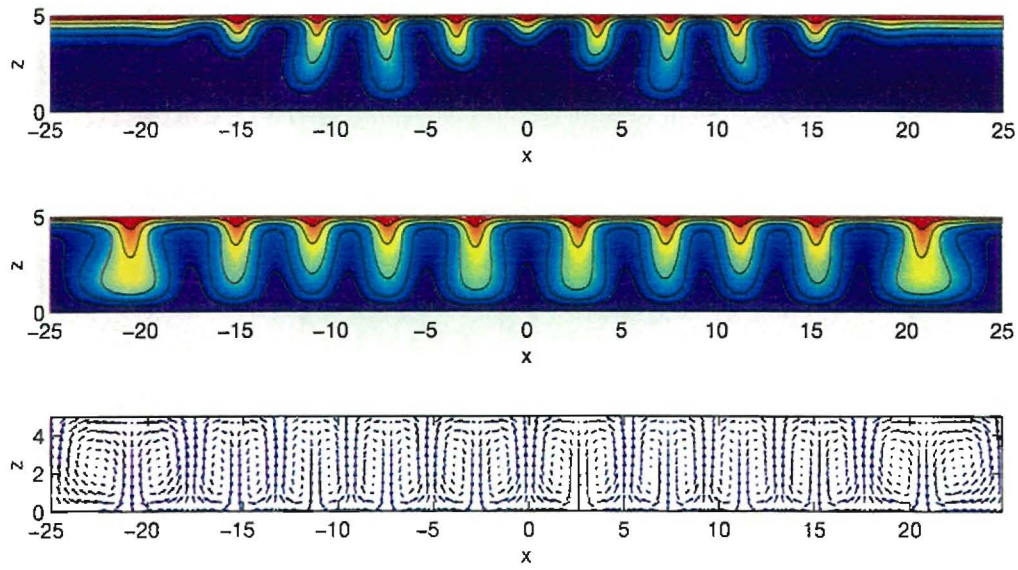

Plate 3. Non-periodic initial perturbation (4.10): saturation profile at $t = 3.5$ (top) and $t = 15$ (middle), velocity field (bottom) at $t = 15$.

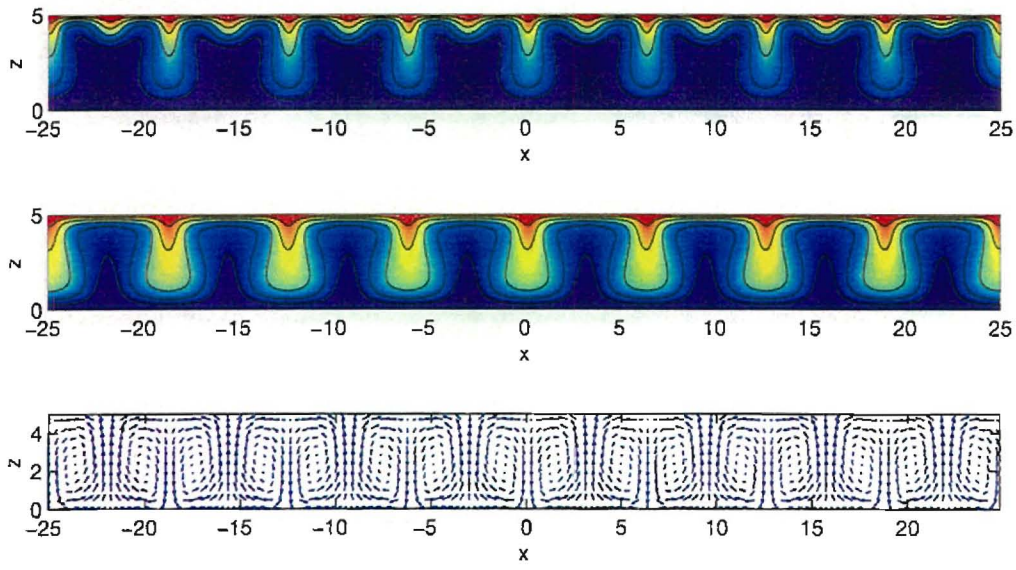

Plate 4. Combined periodic initial perturbation (4.10): saturation profile at $t = 3$ (top) and $t = 15$ (middle), velocity field (bottom) at $t = 15$.

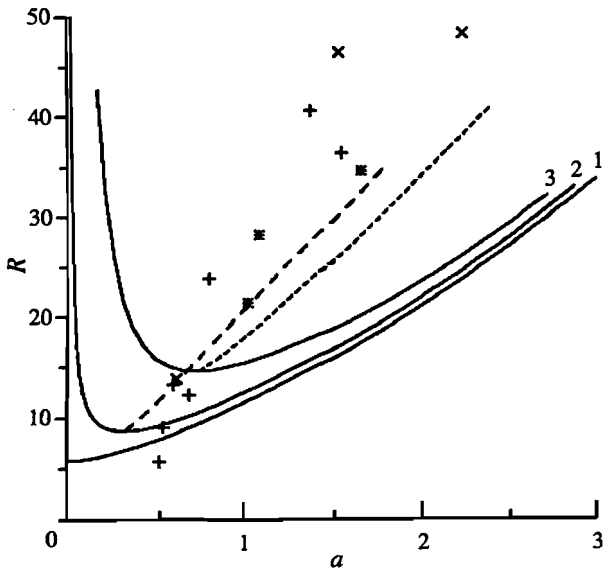

Figure 6. Comparison of theory (this paper) with experimental results (*Wooding et al.* [1997a, b]). Solid curves 1–3 give eigenvalues R versus wavenumber a for the equilibrium boundary layer (Figure 1). Curves of minima of R with respect to a for $t > 0$ increasing to equilibrium: by energy method (Figure 2, dashes), by linearised theory (Figure 3, short dashes). Symbols for experimental results are identified in the text.

fourth order eigenvalue problem which we solved again by the Jacobi–Davidson method. The corresponding stability curves are shown in Figure 3. Now we are in the position to estimate an elapsed time beyond which the boundary layer becomes unstable. This is explained in Section 3.3, see (3.55).

In Section 4 we considered two-dimensional flow and study the growth of instabilities by means of the finite element method (with the stream function as flow variable). Introducing the energy functional (4.8) we are now in a position to estimate the elapsed time numerically for a given initial perturbation. In this way we could qualitatively reproduce Figure 3 (linearised stability) for small periodic perturbations. The response of the system to other initial perturbations was investigated as well. The results are shown in Plate 2 (stochastic), Plate 3 (non-periodic) and Plate 4 (combination of periodic modes). The stochastic case shows a preferential wavenumber which can be estimated in terms of the curves tracing the minima in Figures 2 and 3. It is also worthwhile to note that different initial perturbations may lead to different steady states (occuring at large times). This follows clearly from Figure 4 (right), where the energy functional is plotted versus time.

Figure 6 repeats the equilibrium stability curves of Figure 1 and includes experimental measurements obtained using a tilted Hele–Shaw cell to simulate two-dimensional flow in a porous medium, with inflow of a saline solution and evaporation along part of the upper edge (*Wooding et al.* [1997a, b], *Simmons et al.* [1999]). Experimental points are represented in Figure 6 by the symbols $+$, $\times$ and $*$. In the experiments, the large scale Rayleigh number R_s based on finite "aquifer" depth was greater than 10^2 times the boundary layer R-value. Although the large scale flow in the experimental work differed from a simple vertical upflow, a uniform evaporation rate was modelled and a saline boundary layer of uniform thickness was observed to develop. Wavenumbers of initial instabilities, scaled to the equilibrium boundary layer thickness, were measured for a wide range of R-values. Previously, these observations were plotted by *Wooding et al.* [1997a, Figure 7] using wavenumbers scaled to the diffusion thickness and therefore equivalent to a/R in the present case.

From the published experimental data, stable boundary layers were observed for R-values of 5.8, 5.6 (two experiments), and smaller R. Unstable boundary layers resulted for R-values of 5.6 (one experiment), 8.9 (two experiments), and larger R. Except for the unexplained appearance of instability in one experiment performed at $R = 5.6$, there was a clear separation of stable and unstable layers into two ranges. If the single unstable result at $R = 5.6$ is not included, the theoretical lower bound of 8.590 obtained using the alternative energy method is in agreement with the results of the experimental studies.

The dashed curves in Figure 6 provide traces of the minima of the stability curves defined by the energy method in Figure 2 and by linearised stability analysis in Figure 3. For the data obtained by experimental simulation, either curve might be considered as an upper bound to the wavenumber of an instability which first appears. This is on the assumption that growth rate is zero at a critical point for stability, and a growing perturbation becomes significant when the boundary layer thickness scale has increased significantly. Clearly, however, the instabilities plotted in Figure 6 have been initiated by perturbations of small but finite amplitude, and the energy method with differential constraint provides the appropriate estimate. Three experimental points at the low-R end appear to be exceptional. These occur in a range where accurate observation becomes more difficult, and an inadvertent change of background con-

ditions could have altered the wavenumber.

In general, we may conclude that the alternative formulation of the energy method has improved the quantitative and qualitative estimate of a lower bound to absolute stability, and is in agreement with experimental modelling. The comparison with results from linearised analysis yields interesting qualitative similarities, and stability properties of a growing boundary layer can be described in some detail. The above results have applications to the theory of stability of salt lakes and the salinization of groundwater.

REFERENCES

Abramowitz, M., and I.A. Stegun, *Handbook of Mathematical Functions*, Dover, 1972.

Bear, J., *Dynamics of Fluids in Porous Media*, Elsevier, New York, 1972.

Caltagirone, J.-P., Stability of a saturated porous media layer subject to a sudden rise in surface temperature: comparison between the linear and energy methods, *Quart. J. Mech. Appl. Math.*, *33*, 47–58, 1980.

Davis, S. H., On the possibility of supercritical instabilities, in *Instability of Continuous Systems, Proc. IUTAM Symp.*, pp. 222–227, Springer–Verlag, Berlin, 1971

De Josselin de Jong, G., Singularity distributions for the analysis of multiple fluid flow in porous media, *J. Geothermal Res.*, *65*, pp. 3739–3758, 1960

Fokkema, D. R., G. L. G. Sleijpen and H. A. van der Vorst, Jacobi–Davidson style QR and QZ algorithms for the reduction of matrix pencils, *SIAM J. Sci. Comput.*, *20*, 94–125, 1999.

Gilman, A and J. Bear, The influence of free convection on soil salinization in arid regions, *Transport in Porous Media*, *24*, 275–301, 1996.

Homsy, G. M., Global stability of time-dependent flows: impulsively heated or cooled fluid layers, *J. Fluid Mech.*, *60*, 129–139, 1973.

Homsy, G. M., A. E. Sherwood, Convective instabilities in porous media with throughflow, *Lawrence Livermore Lab. Rep.*, UCRL-76539, 1975.

Homsy, G. M., A. E. Sherwood, Convective instabilities in porous media with throughflow, *Amer. Inst. Chem. Engrs. J.*, *22*, 168–174, 1976.

Jones, M. C. and J. M. Persichetti, Convective instability in packed beds with throughflow, *Amer. Inst. Chem. Engrs. J.*, *32*, 1555–1557, 1986.

Lapwood, E. R., Convection of a fluid in a porous medium, *Proc. Cambridge Phil. Soc.*, *44*, 508–521, 1948.

Nield, D. A., Convective instability in porous media with throughflow, *Amer. Inst. Chem. Engrs. J.*, *33*, 1222-1224, 1987.

Nield, D. A., A. Bejan, *Convection in Porous Media*, 2nd ed., Springer–Verlag, New York, 1992.

Pieters, G. J. M., Stability analysis for a saline boundary layer formed by uniform upflow using finite elements, *RANA Report 01-07*, Eindhoven University of Technology, 2001.

Simmons, C. T., K. A. Narayan and R. A. Wooding, On a test case for density-dependent groundwater flow and solute transport models: The salt lake problem, *Water Resources Res.*, *35*(12), 3607–3620, 1999.

Sleijpen, G. L. G., H. A. van der Vorst, A Jacobi–Davidson iteration method for linear eigenvalue problems, *SIAM J. Matrix Anal. Appl.*, *17*(2), 401–425, 1996.

Straughan, B., *The Energy Method, Stability and Nonlinear Convection*, vol. 91 of *Applied Mathematical Sciences*, Springer–Verlag, New-York, 1992.

Temam, R., *Navier–Stokes Equations, Theory and Numerical Analysis*, vol. 2 of *Studies in Mathematics and its Applications*, 3rd ed., Elsevier Science Publishers, Amsterdam, 1984.

Van Duijn, C. J., R. A. Wooding, and A. van der Ploeg, Stability criteria for the boundary layer formed by throughflow at a horizontal surface of a porous medium: extensive version, *RANA Report 01-05*, Eindhoven University of Technology, 2001.

Wooding, R. A., Rayleigh instability of a thermal boundary layer in flow through aporous medium, *J. Fluid Mech.*, *9*, 182–192, 1960.

Wooding, R. A., S. W. Tyler, and I. White, Convection in groundwater below and evaporating salt lake: 1. Onset of instability, *Water Resour. Res.*, *33*(6), 1199–1217, 1997a.

Wooding, R. A., S. W. Tyler, I. White, and P. A. Anderson, Convection in groundwater below and evaporating salt lake: 2. Evolution of fingers or plumes, *Water Resour. Res.*, *33*(6), 1219–1228, 1997b.

C. J. van Duijn, Department of Mathematics and Computer Science, Eindhoven University of Technology, P.O. Box 513, 5600 MB Eindhoven.

G. J. M. Pieters, Department of Mathematics and Computer Science, Eindhoven University of Technology, P.O. Box 513, 5600 MB Eindhoven.

A. van der Ploeg, MARIN, P.O. Box 28, 6700 AA Wageningen, The Netherlands.

R. A. Wooding, CSIRO Land and Water, G.P.O. Box 1666, Canberra, ACT 2601, Australia.

APPENDIX A

In this appendix we compare the maximum problem (3.12) for the admissible perturbations $\mathbf{H}$ and $\widetilde{\mathbf{H}}$. In particular we show that $\widetilde{\mathbf{H}}$ can be identified with a proper subspace of $\mathbf{H}$. This explains why the differential constraint yields larger Rayleigh numbers than the integral constraint.

Let $(s, w) \in \widetilde{\mathbf{H}}$. For this given s we have the unique

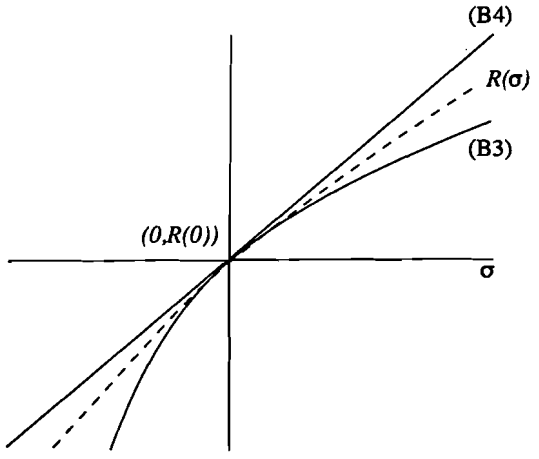

Figure B1. Behaviour of eigenvalues $R(\sigma)$ (linearised stability) near $\sigma = 0$.

decomposition (*Temam* [1984])

$$se_z = \boldsymbol{v} + \text{grad}\,\varphi \quad (\boldsymbol{v}, \varphi \text{ are } x,y\text{-periodic}), \qquad \text{(A1)}$$

where div $\boldsymbol{v} = 0$ and $\boldsymbol{v} \cdot \boldsymbol{n} = 0$ on $\partial\mathcal{V}$. Here $\boldsymbol{n}$ denotes the unit normal at the boundary $\partial\mathcal{V}$. As in (3.5) we find

$$\Delta v_3 = \Delta_\perp s \quad \text{in } \mathcal{V},$$

where v_3 is the vertical component of $\boldsymbol{v}$. This implies

$$\Delta(v_3 - w) = 0 \quad \text{in } \mathcal{V},$$

and the boundary conditions on $\partial\mathcal{V}$ give $v_3 = w$ in $\mathcal{V}$. Thus given $(s,w) \in \widetilde{\mathbf{H}}$ we have obtained the pair $(s,\boldsymbol{v})$ with div $\boldsymbol{v} = 0$ and $v_3 = w$ in $\mathcal{V}$. Multiplying (A1) by $\boldsymbol{v}$ and integrating the result over $\mathcal{V}$ gives

$$\int_{\mathcal{V}} |\boldsymbol{v}|^2 = \int_{\mathcal{V}} sw,$$

in other words, $(s,\boldsymbol{v}) \in \mathbf{H}$.

The converse is not true. Given $(s,\boldsymbol{u}) \in \mathbf{H}$ and using (A1) we obtain the vector field $\boldsymbol{v}$ satisfying $\Delta v_3 = \Delta_\perp s$ in $\mathcal{V}$. So $(s,v_3) \in \widetilde{\mathbf{H}}$, but in general $\boldsymbol{v} = \boldsymbol{u} + \text{curl}\,\boldsymbol{\Phi}$ for a smooth vector field $\boldsymbol{\Phi}$ which vanishes on $\partial\mathcal{V}$.

APPENDIX B

Let $a > 0$ and $t > 0$ be fixed. To simplify notation we set $r = -a^2\partial S_0/\partial z$. Note that $r = r(a,z,t) > 0$ for all $z > 0$. Combining (3.48), (3.49) and (3.52) yields the eigenvalue problem

$$L_\sigma w := (D^2 + D - a^2 - \sigma)(D^2 - a^2)w = rRw$$

for $0 < z < \infty$, with

$$w(0) = D^2w(0) = 0, \qquad w(\infty) = 0.$$

Let $R(\sigma) := R_1(a,t,\sigma)$ denote the smallest positive eigenvalue and w_σ the corresponding eigenfunction. We want to show

$$R(\sigma) \lesseqgtr R(0) \text{ if and only if } \sigma \lesseqgtr 0. \qquad \text{(B1)}$$

Note that

$$L_\sigma = L_0 - \sigma(D^2 - a^2).$$

Below we denote by $(\cdot,\cdot)$ the L^2-inner product and by $||\cdot||$ the induced norm. Since $L_\sigma w_\sigma = rR(\sigma)w_\sigma$ we have

$$(L_\sigma w_\sigma, w_\sigma) = R(\sigma)(rw_\sigma, w_\sigma)$$

or

$$(L_0 w_\sigma, w_\sigma) + \sigma\{||Dw_\sigma||^2 + ||w_\sigma||^2\} = R(\sigma)(rw_\sigma, w_\sigma). \qquad \text{(B2)}$$

Since

$$R(0) = \inf_W \frac{(L_0 w, w)}{(rw,w)} \le \frac{(L_0 w_\sigma, w_\sigma)}{(rw_\sigma, w_\sigma)}$$

where W is a suitably chosen function space, we obtain from (B2) the estimate

$$R(\sigma) - R(0) \ge \sigma \frac{||Dw_\sigma||^2 + ||w_\sigma||^2}{(rw_\sigma, w_\sigma)}. \qquad \text{(B3)}$$

Using $L_0 w_0 = rR(0)w_0$ or

$$L_\sigma w_0 + \sigma(D^2 - a^2)w_0 = rR(0)w_0,$$

we find in a similar fashion the upperbound

$$R(\sigma) - R(0) \le \sigma \frac{||Dw_0||^2 + ||w_0||^2}{(rw_0, w_0)}. \qquad \text{(B4)}$$

This proves (B1) and thus (3.50) for σ sufficiently small. Note that (B3) and (B4) imply

$$\left.\frac{\mathrm{d}R}{\mathrm{d}\sigma}\right|_{\sigma=0} = \frac{||Dw_0||^2 + ||w_0||^2}{(rw_0, w_0)} > 0. \qquad \text{(B5)}$$

To conclude this appendix, we show that the lower bound in (B3) is a concave function of σ near $\sigma = 0$. Differentiating $L_\sigma w_\sigma = rR(\sigma)w_\sigma$ with respect to σ and setting $v_\sigma := \mathrm{d}w_\sigma/\mathrm{d}\sigma$ gives

$$L_\sigma v_\sigma - (D^2 - a^2)w_\sigma = rR(\sigma)v_\sigma + r\frac{\mathrm{d}R}{\mathrm{d}\sigma}w_\sigma,$$

implying

$$(L_\sigma v_\sigma - rR(\sigma)v_\sigma, v_\sigma) + (Dv_\sigma, Dw_\sigma) + a^2(v_\sigma, w_\sigma) = \frac{\mathrm{d}R}{\mathrm{d}\sigma}(v_\sigma, rw_\sigma) .$$

Since $(v_\sigma, w_\sigma) = \frac{1}{2}\frac{\mathrm{d}}{\mathrm{d}\sigma}||w_\sigma||^2$ (other terms similarly) and since $(L_\sigma v_\sigma - rR(\sigma)v_\sigma, v_\sigma) > 0$ (assuming v_σ not in the eigenspace spanned by w_σ), we obtain the differential inequality

$$\frac{\mathrm{d}}{\mathrm{d}\sigma}\{||Dw_\sigma||^2 + ||w_\sigma||^2\} < \frac{\mathrm{d}R}{\mathrm{d}\sigma}\frac{\mathrm{d}}{\mathrm{d}\sigma}(rw_\sigma, w_\sigma) \qquad \text{(B6)}$$

for all σ, and in particular for $\sigma = 0$.

Next set

$$F(\sigma) = \frac{||Dw_\sigma||^2 + ||w_\sigma||^2}{(rw_\sigma, w_\sigma)} .$$

Differentiating this expression and using (B6), (B5) results in

$$\left.\frac{\mathrm{d}F}{\mathrm{d}\sigma}\right|_{\sigma=0} < 0 .$$

Moreover, since

$$\frac{\mathrm{d}^2}{\mathrm{d}\sigma^2}(\sigma F(\sigma)) = 2\frac{\mathrm{d}F}{\mathrm{d}\sigma} + \sigma\frac{\mathrm{d}^2F}{\mathrm{d}\sigma^2} ,$$

we find

$$\left.\frac{\mathrm{d}^2}{\mathrm{d}\sigma^2}(\sigma F(\sigma))\right|_{\sigma=0} < 0 ,$$

which implies the concavity of the lower bound in (B3) near $\sigma = 0$. Thus for small $|\sigma|$ the eigenvalues $R(\sigma)$ behave as in Figure B1.